Letter

Magnetization process and ordering of the $S = \frac{1}{2}$ pyrochlore Heisenberg antiferromagnet in a magnetic field

Imre Hagymási [1,2,*] Robin Schäfer [1,†] Roderich Moessner,[1,‡] and David J. Luitz [1,§]

[1]*Max Planck Institute for the Physics of Complex Systems, Noethnitzer Strasse 38, 01187 Dresden, Germany*

[2]*Strongly Correlated Systems "Lendület" Research Group, Institute for Solid State Physics and Optics, Wigner Research Centre for Physics, P.O. Box 49, H-1525 Budapest, Hungary*

(Received 6 August 2021; revised 11 July 2022; accepted 18 July 2022; published 31 August 2022)

We study the $S = \frac{1}{2}$ pyrochlore Heisenberg antiferromagnet in a magnetic field. Using large-scale density-matrix renormalization group calculations for clusters with up to 128 spins, we find indications of a finite triplet gap, causing a threshold field to nonzero magnetization in the magnetization curve. We obtain a robust saturation field consistent with a magnon crystal, although the corresponding 5/6 magnetization plateau is very slim and possibly unstable. Most remarkably, there is a pronounced and apparently robust 1/2 magnetization plateau where the ground state breaks the rotational symmetry of the lattice, exhibiting *oppositely polarized* spins on alternating kagome and triangular planes. Reminiscent of the kagome ice plateau of the pyrochlore Ising antiferromagnet known as spin ice, it arises via a much more subtle "quantum order by disorder" mechanism.

DOI: 10.1103/PhysRevB.106.L060411

Introduction. The Heisenberg antiferromagnet on the pyrochlore lattice is one of the most frustrated three-dimensional magnets and, as such, a prime candidate for exotic, specifically quantum spin liquid, behavior. Indeed, its classical variants are topological magnets (classical spin liquids), exhibiting a Coulomb phase [1–3] in the limit of low temperature for both the Heisenberg [4] and Ising (spin ice) variants, with the latter also hosting deconfined magnetic monopoles as quasiparticles [5–8].

Due to the complexity of the quantum $S = \frac{1}{2}$ problem and concomitant lack of unbiased methods, the nature of the ground state of the pyrochlore Heisenberg antiferromagnet is still being discussed [9–18], with recent progress indicating that the ground state breaks inversion symmetry [19–21] rather than being a quantum spin liquid.

In a related strand of work, the study of frustrated magnets in an applied field [22] has turned up many interesting phenomena, such as string excitations and Kasteleyn transitions, dimensional reduction, and much more. Particularly prominent has been the study of magnon crystals [23–29] and the magnetization plateau [24,30–37], "incompressible" magnetic states which may be stabilized when gaps between the ground states of different magnetization sectors remain finite in the thermodynamic limit.

The classical variants exhibit either no magnetization plateau for the Heisenberg model (at least in the absence of magnetoelastic coupling [37–39]) or, in the Ising case, the very rich physics of kagome ice [40–42]. The latter arises for a field applied in a [111] direction, which has a large projection onto the local Ising axes on one quarter of the spins, which therefore quickly get polarized. The remaining three quarters of the spins reside on kagome layers which enter a stable partially polarized plateau at intermediate field strengths.

In the quantum limit, this magnetization process remains largely unexplored [36,43–46], precisely due to the lack of reliable methods alluded to above, while the two-dimensional $S = \frac{1}{2}$ kagome Heisenberg antiferromagnet has been thoroughly studied [24,27–35,47,48]. Although a material which

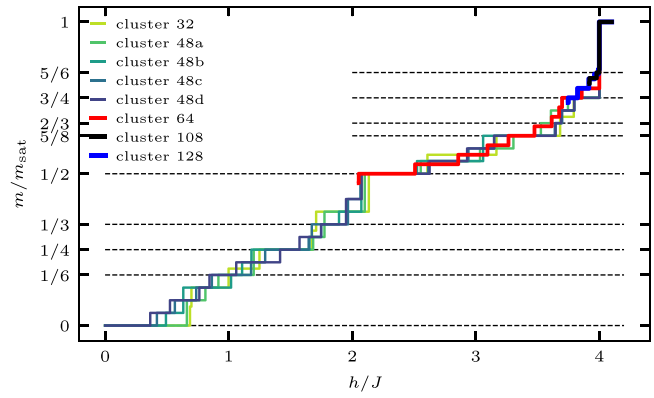

FIG. 1. Normalized ground state magnetization $m = \langle \psi_0 | S^z_{\rm tot} | \psi_0 \rangle$ of different pyrochlore clusters as a function of the external magnetic field h. The saturation magnetization is given by the fully polarized state of N spins: $m_{\rm sat} = N/2$. For the 64-site cluster the upper half of the curve can be reliably calculated, while for the largest clusters, 108 and 128, only the part of the curve at the strongest fields can be reliably calculated.

*hagymasi@pks.mpg.de
†schaefer@pks.mpg.de
‡moessner@pks.mpg.de
§dluitz@pks.mpg.de

can be modeled by an SU(2) symmetric $S = \frac{1}{2}$ Heisenberg model is still lacking, higher-spin Heisenberg materials are known, such as the $S = 1$ compound $NaCaNi_2F_7$ [49] and the $S = \frac{3}{2}$ compound $CdCr_2O_4$. In the latter compound a robust $\frac{1}{2}$ magnetization plateau has been observed [38].

Here, we study the magnetization process of the $S = \frac{1}{2}$ Heisenberg antiferromagnet from zero field to saturation using the density-matrix renormalization group (DMRG), which recently turned out to be very useful in regard to the zero-field properties [19]. Most saliently, we find an incompressible magnetic phase with a 3:1 spin polarization ratio, signaled by a robust plateau at half saturation.

The ground state corresponding to this plateau breaks the rotational symmetry of the lattice. It exhibits polarized kagome planes along the field direction and *anti*polarized interplane sites. Unlike in kagome ice, this pattern of 3:1 disproportionation arises spontaneously, being selected from an exponentially large number of possible 3:1 disproportionations in what may be termed a quantum order by disorder mechanism. Also, the minority sublattice has *negative*, rather than enhanced, Zeeman energy—a spontaneous instance of ferrimagnetism.

Furthermore, we obtain a value of the saturation field which is consistent with what one obtains for the magnon crystal state, an exact eigenstate of a range of frustrated Heisenberg magnets [25].

Methods. We determine the field dependence of the ground state magnetization for periodic clusters ranging from $N = 32$ to $N = 128$ spins, using SU(2) and U(1) DMRGs [50–53]. Although the DMRG is, by nature, a one-dimensional method [54–58], it has been successfully used in two [59] and, recently, three dimensions [19,60] by linearizing the system along a snake's path at the price of nonlocal interactions within the snake. Conservation of the total spin S_{tot} and its z component S^z_{tot} allows us to target and optimize the ground states within the concomitant symmetry sectors. We observe that despite the fact that the SU(2) representation is very efficient in higher-spin sectors, the convergence while optimizing the energy is sometimes better when explicitly enforcing only the U(1) spin symmetry. Since the wave function is represented as a matrix-product state with finite bond dimension, extrapolation to infinite bond dimension is necessary. This is usually done by extrapolating as a function of either the truncation error or the variance [57]. We optimize the wave function for small bond dimensions ($\lesssim$2000) using the two-site DMRG algorithm, but for larger bond dimensions we switch to the single-site variant with subspace expansion [52]. For the bond dimensions we used [up to ∼20 000 SU(2) or U(1) states] the calculation of the full variance is impractical, and we therefore extrapolate these energies to the error-free limit as a function of the two-site variance. This quantity was shown to be equally good compared to the truncation error [61]; see Appendix A for further details.

Magnetization curve. We consider the ground state of the $S = \frac{1}{2}$ pyrochlore Heisenberg antiferromagnet

$$H = J \sum_{\langle i,j \rangle} \vec{S}_i \cdot \vec{S}_j - h \sum_i S^z_i \qquad (1)$$

in a finite magnetic field, $h > 0$. The spins are located on a pyrochlore lattice defined by the fcc lattice vectors $\vec{a}_1 = \frac{1}{2}(1, 1, 0)^T$, $\vec{a}_2 = \frac{1}{2}(1, 0, 1)^T$, and $\vec{a}_3 = \frac{1}{2}(0, 1, 1)^T$, together with four tetrahedral basis vectors, $\vec{b}_0 = 0$ and $\vec{b}_i = \frac{1}{2}\vec{a}_i$. This model conserves the total magnetization $S^z_{\text{tot}} = \sum_i S^z_i$ since $[H, S^z_{\text{tot}}] = 0$, and hence, the Hamiltonian decomposes into symmetry sectors with fixed total magnetization $m = -N/2, -N/2 + 1 \cdots N/2$. This means that each eigenstate $|n\rangle_m$ of H is also an eigenstate of S^z_{tot}: $S^z_{\text{tot}}|n\rangle_m = m|n\rangle_m$, and therefore, the eigenstates of the Hamiltonian are *independent* of the field h, and their energy $E^n_m(h)$ is shifted with respect to the zero-field value $E^n_m(0)$ by $E^n_m(h) = E^n_m(0) - hm$.

In the absence of a field, $h = 0$, the ground state of the Hamiltonian is in the $m = 0$ sector. For finite values of $h > 0$, the energies of states exhibiting a finite magnetization $m \neq 0$ will change by $-hm$ and potentially become the overall ground state of the system. This leads to the characteristic jumps of the magnetization in Fig. 1. The field strength at which a transition of the ground state magnetization from m to $m + 1$ occurs is entirely determined by the minimal energy of all states in sectors m and $m + 1$ *in the absence of the field*, $E^0_m(h = 0) = \min_n E^n_m(h = 0)$. The field where $E^0_{m+1}(h)$ becomes lower than $E^0_m(h)$ is determined by $E^0_{m+1}(h) = E^0_m(h)$, i.e.,

$$E^0_{m+1}(h = 0) - h(m + 1) = E^0_m(h = 0) - hm, \qquad (2)$$

which is solved by $h = E^0_{m+1}(h = 0) - E^0_m(h = 0)$. Multiple transitions between m, $m + 1$, $m + 2$, ... can coincide, leading to a larger change at a given field strength. To obtain the full magnetization curve for a given cluster, we therefore have to calculate the lowest energies in all magnetization sectors at zero field using the DMRG, respecting the $U(1)$ symmetry associated with the conservation of S^z_{tot}. In fact, since the total spin S^2_{tot} also commutes with both H and S^z_{tot}, we can also use the full SU(2) symmetry as mentioned above.

If the ground states of adjacent S^z_{tot} sectors are separated by a gap in the thermodynamic limit, the magnetization will remain locked into the lower magnetization sector for a range of fields proportional to the gap, leading to a plateau in the magnetization curve and hence an incompressible magnetic state.

We display the resulting magnetization curves in Fig. 2 for different clusters ranging from 32 to 128 sites as shown in Table I. Please note that for large clusters it is possible to determine only the large-field part of the magnetization curve.

A prominent feature is the large jump of the magnetization from its maximum to $5/6\, m_{\text{sat}}$ near the saturation field $h_{\text{sat}} = 4J$. The position and height of this jump can be understood using the same reasoning as in the case of kagome [28,31]. The exact ground state of symmetry sectors with very large S^z_{tot} is a crystal of localized magnon modes, while the ground state of the sector with maximal S^z_{tot} is the trivial fully polarized state. One of the densest packings of independent magnon modes on the pyrochlore lattice possible is given by densely arranging magnons localized on hexagonal motifs in the kagome planes, leading to a magnetization plateau at $m/m_{\text{sat}} = 5/6$ (see Appendix B for details). Each magnon mode reduces the energy by $4J$, so that $h_{\text{sat}} = 4J$ [Eq. (B4)]. Each independent magnon excitation requires three unit cells (12 sites), which

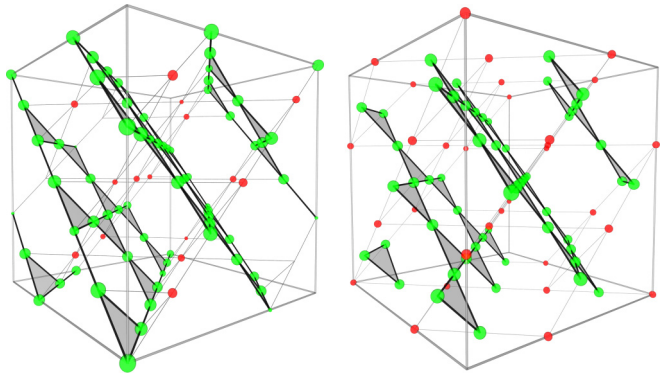

FIG. 2. On-site magnetization for the $m/m_S = \frac{1}{2}$ plateau of the 108-site and 128-site clusters. We show only the cubic unit cell cut of the clusters for better comparison. Green balls correspond to polarized spins in one direction; red balls represent a polarization in the opposite direction. The size of the balls is proportional to the on-site magnetization. Gray shaded triangles are a guide to the eye to indicate the polarized kagome planes.

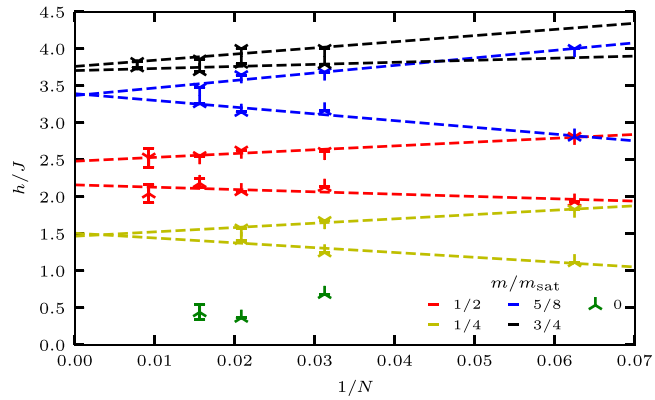

FIG. 3. Extrapolation to the thermodynamic limit of magnetization jumps for the plateaus $m/m_{\rm sat} = 1/2$ (red), 5/8 (blue), and 3/4 (black) based on simple linear fits in $1/N$. The lower (h_-) and higher (h_+) points of each plateau define the jump towards lower and higher magnetization plateaus for different cluster sizes, respectively. We obtained the following values in the thermodynamic limit: $h_+^{1/2} = 2.48(1)J$, $h_-^{1/2} = 2.16(5)J$. To gain further data points for the finite-size scaling we included a cluster given by four unit cells (16 sites) with periodic boundary conditions.

fixes the densest packing. Due to the requirement of commensurability of the densest packing with the cluster geometry, we find the $\frac{5}{6}$ plateau only for the 108-site cluster in Fig. 1. On other clusters we can obtain even larger jumps at $h = 4J$, as modes localized on shorter loops winding across periodic boundary conditions can yield a denser magnon mode filling as a finite-size effect. This yields, for the 32- and 48-site clusters, a broad plateau at $m/m_{\rm sat} = 3/4$ which is not representative of the infinite lattice. The narrowness of the $\frac{5}{6}$ plateau on the 108-site cluster in turn calls into question its stability in the thermodynamic limit.

We attempt to extrapolate the widths of the magnetization plateau observed in finite size clusters (Fig. 1) to the thermodynamic limit (Fig. 3), using linear fits in $1/N$. There is little indication that the $\frac{3}{4}$ and $\frac{5}{8}$ plateaus retain a finite width. In contrast, we have strong evidence for a finite width of the $\frac{1}{2}$ plateau in the thermodynamic limit (red in Fig. 3), which is located in the field range $h_-^{1/2} \leqslant h \leqslant h_+^{1/2}$, with jumps at $h_-^{1/2} = 2.16(5)J$ and $h_+^{1/2} = 2.48(1)J$. The size of the zero plateau (determined by the triplet gap) varies nonmonotonically with cluster size and geometry and is inaccessible for our largest clusters, rendering a smooth extrapolation impossible. Nevertheless, our result for the triplet gap in the 64-site cluster, 0.42(11), agrees with that of the recent variational Monte Carlo estimate, 0.40(4), in the thermodynamic limit [21], and the data shown in Fig. 3 are consistent with a finite triplet gap.

It is worth commenting on the actual values of the magnetic field to make the comparison with experiments easier. Since a material which realizes the $S = \frac{1}{2}$ Heisenberg model is still lacking, the closest relative we can consider is the $S = 1$ compound $NaCaNi_2F_7$ [49]. Assuming the same value of $J \sim 3.2$ meV in a $S = \frac{1}{2}$ material (and g factor $g \sim 2$), the saturation field would correspond to $B_{\rm sat} \sim 110$ T, and the $\frac{1}{2}$ plateau is expected to start at ~68 T. Such high values of magnetic fields are accessible in pulsed field experiments.

Properties of the $\frac{1}{2}$ plateau. We turn to the correlations of the $\frac{1}{2}$ plateau. We focus on the largest cluster, where finite-size effects due to short loops winding across periodic boundaries are suppressed. Nonetheless, we include results for smaller clusters for finite-size extrapolations, as in the preceding analysis. Indeed, while the 32-site cluster develops a uniform magnetization throughout the lattice with $\langle\psi_0|S_i^z|\psi_0\rangle \equiv 0.25$, larger clusters exhibit a more complex pattern, stabilizing inequivalent spins with differing polarization. These are arranged with respect to one of the four rotational axes defined within each tetrahedron. The planes perpendicular to this axis are alternating triangular and kagome planes, containing $\frac{1}{4}$ and $\frac{3}{4}$ of the spins, shown in red and green in Fig. 2, respectively: each tetrahedron contributes a "base triangle" to the kagome plane and its apex spin to the triangular plane.

The kagome spins (A sites in Table II) acquire polarization along the field, while the triangular spins (B sites) are polarized *in the opposite direction* in our clusters of size 64, 108, and 128. Figure 2 shows the on-site magnetization

TABLE I. Cluster vectors $\vec{c}_1$, $\vec{c}_2$, and $\vec{c}_3$ for the eight clusters used in this work. The last column shows the length of the shortest loop winding across the periodic boundary and thus competing with the loops in the bulk (e.g., hexagons of length 6). The clusters of size 32 and 108 respect all lattice symmetries.

Cluster	$\vec{c}_1$	$\vec{c}_2$	$\vec{c}_3$	Length
32	$2\vec{a}_1$	$2\vec{a}_2$	$2\vec{a}_3$	4
48a	$(\frac{3}{2}, \frac{1}{2}, 0)^T$	$(0, 1, 1)^T$	$(0, 1, -1)^T$	4
48b	$(\frac{3}{2}, \frac{1}{2}, 0)^T$	$(0, \frac{1}{2}, \frac{3}{2})^T$	$(0, 1, -1)^T$	4
48c	$(\frac{3}{2}, 1, \frac{1}{2})^T$	$(0, 1, -1)^T$	$(1, -1, 0)^T$	4
48d	$(1, 1, 1)^T$	$(1, 0, -1)^T$	$(1, -1, 0)^T$	4
64	$(1, 1, 1)^T$	$(1, 1, -1)^T$	$(-1, 1, 1)^T$	6
108	$3\vec{a}_1$	$3\vec{a}_2$	$3\vec{a}_3$	6
128	$(2, 0, 0)^T$	$(0, 2, 0)^T$	$(0, 0, 2)^T$	8

TABLE II. Averaged on-site magnetization $\langle S_i^z \rangle$ and standard deviation across sites of the two types of sites, A and B, observed in the finite cluster with size N. We excluded the defects (9 of $N = 64$, 6 of $N = 108$, and 0 of $N = 128$) in the form of the lines with small on-site magnetization to determine the averaged values.

N	A	B
64	0.379 ± 0.077	-0.161 ± 0.000
108	0.419 ± 0.036	-0.245 ± 0.044
128	0.426 ± 0.015	-0.278 ± 0.007

pattern $\langle \psi_0 | S_i^z | \psi_0 \rangle$ in a cubic unit cell for clusters of sizes 108 and 128, along with a list for different clusters in Table II. While the largest cluster with 128 sites develops this pattern perfectly, smaller clusters can exhibit defects in the form of lines with small on-site magnetization passing through kagome planes, which we attribute to the existence of short resonant loops across the periodic boundaries in these clusters. The number of such defective sites is listed in the caption of Table II and vanishes for the 128-site cluster.

We emphasize that this symmetry breaking is distinct from the one we found for the zero-field problem, where the lattice inversion symmetry appears to be broken, as the two sublattices of tetrahedrons have different energy densities [19]. On the $\frac{1}{2}$ magnetization plateau, the inversion symmetry is preserved, while the rotational symmetry of the lattice is broken by the emergence of a preferred [111] axis. The rotational symmetry around this axis is not broken, but those within the three other kagome planes are.

The symmetry breaking is naturally reflected in the spin structure factor

$$S(\vec{Q}) = \frac{4}{3N} \sum_{ij} \langle \vec{S}_i \cdot \vec{S}_j \rangle_c \cos[\vec{Q} \cdot (\vec{R}_i - \vec{R}_j)], \qquad (3)$$

where $\vec{R}_i$ denote the real-space coordinates of sites and the index c denotes the connected part of the correlation matrix (the factor $\frac{4}{3}$ comes from normalization $1/[S(S+1)]$ for spin $S = \frac{1}{2}$). This is plotted in Fig. 4 for several clusters. The larger clusters exhibit clearly discernible bright lines in the structure factor, discarding the rotational symmetry present for the 32-site cluster; in contrast to the $m/m_s = 0$ state, the inversion symmetry remains intact.

Earlier work [43] predicted another possible pattern, the R state, for the $S = \frac{3}{2}$ case. We discuss the competition of the R state with the best variational wave function in Appendix A and conclude that the R state has higher energy.

Discussion. The pyrochlore Heisenberg antiferromagnet in a field, like its zero-field cousin, illustrates the capacity of frustrated magnets to exhibit a plethora of instabilities, discarding the rotational symmetry at half magnetization and forming an incompressible state. It is interesting to embed this finding in a broader context.

First, the idea that the half-magnetization plateau goes along with a 3:1 disproportionation of sites seems entirely natural: indeed, for collinear spins, such a 3:1 ratio is the only way to obtain half-magnetized tetrahedrons. Note, however, that such 3:1 tetrahedrons can be tiled in exponentially numerous ways on the pyrochlore lattice, indeed mapping onto dimer coverings of the diamond lattice, which have a finite entropy of $S \approx 0.13 k_B$ [62–64]. The selection through fluctuations of a specific one (or subset) of such tilings with lowered symmetry is known as order by disorder. In this sense, our magnetization plateau exhibits a form of quantum order by disorder, although the assignment of what term of the Hamiltonian contributes the fluctuations is to some degree a matter of choice. At any rate, the emergence of ordered ferrimagnetism in the plateau is a striking instability of a highly frustrated quantum magnet.

We close by contrasting the $\frac{1}{2}$ plateau to the kagome ice plateau mentioned in the Introduction. In a real pyrochlore material with spin-orbit coupling, an Ising anisotropy needs to go along with noncollinear easy axes: the local easy axis is the [111] direction joining a site with the centers of its

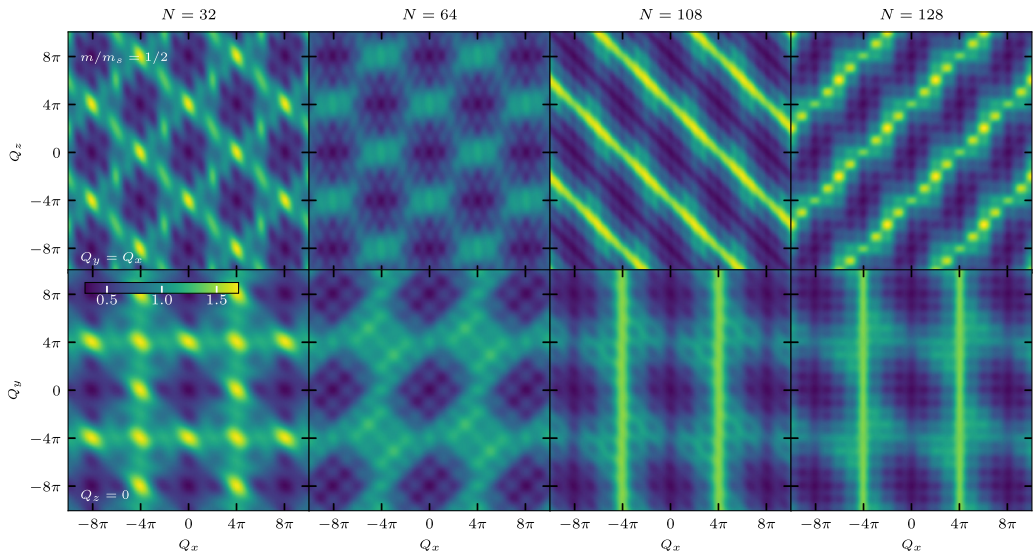

FIG. 4. Spin structure factor $S(\vec{Q})$ for the $m/m_S = \frac{1}{2}$ plateau of various clusters. The top row shows the $Q_y = Q_x$ cut through the Brillouin zone; the bottom row corresponds to the $Q_z = 0$ cut.

tetrahedrons. This turns a uniform applied magnetic field into a staggered Zeeman field according to the sublattice [65]; as mentioned above, when applied along a [111] direction, it polarizes the triangular planes more strongly than the kagome ones, as the easy axis projections differ by a factor of 3. We find it most intriguing that this general setting arises for the $S = \frac{1}{2}$ Heisenberg plateau by spontaneous rather than explicit symmetry breaking, and the question of interpolating between the two immediately poses itself. Note that the two cases differ considerably in (nonsymmetry) "details": the triangular layers are strongly positively polarized in kagome ice, in contrast to their weak *negative* polarization in the Heisenberg $S = \frac{1}{2}$ plateau.

There clearly remains much further scope for studying the highly frustrated quantum magnets in $d = 3$ with and without applied fields, and for the foreseeable future, recent technological progress promises to yield previously inaccessible interesting data such as those underpinning the present paper.

Acknowledgments. We acknowledge support from the Deutsche Forschungsgemeinschaft through SFB 1143 (Project No. 247310070) and Cluster of Excellence ct.qmat (EXC 2147, Project No. 390858490). I.H. was supported in part by the Hungarian National Research, Development and Innovation Office (NKFIH) through Grants No. K120569 and No. K134983. Some of the data presented here were produced using the SYTEN toolkit [50,51].

APPENDIX A: FURTHER DETAILS OF THE DMRG SIMULATION

Matrix-product operators (MPOs) can be constructed by hand for the simplest one-dimensional models with nearest-neighbor interactions. However, this task becomes difficult when long-range interactions are present and needs to be done in an automatic way. While the corresponding MPO of a single product, e.g., $S_i^z S_j^z$, can be represented by an MPO of small bond dimension, the bond dimension grows exponentially by summing up multiple terms. Luckily, the MPO can be compressed effectively using the deparallelization method [66] without any information loss in many cases. We start by optimizing a random matrix-product state with the corresponding size of the cluster using DMRG where the long-range correlations are captured automatically up to a given bond dimension. The choice of the three-dimensional to one-dimensional mapping can influence the overall convergence as well as the final bond dimension of the MPO, which can also have an impact on the speedup of the calculation. However, we did not observe a significant difference in terms of computation time and convergence properties for the different paths in the three-dimensional clusters we investigated.

The convergence problems in three dimensions are even more severe than in two dimensions since there are more periodic bonds yielding to increasing long-range interaction. While we do not face convergence problems for the 32- and 48-site clusters, the DMRG often exhibits bad convergence and gets stuck in local minima for the larger clusters due to its local-update nature. In these cases, the pattern in Fig. 2 is only partially generated if we initialize the algorithm with random states. This can be monitored by examining either the truncation error or the two-site variance as a function of the bond dimension. Metastable states induce a nonmonotonic behavior of these quantities; that is, the energy decreases, but the truncation error or two-site variance increases. When the convergence is smooth, the energy typically follows a linear behavior as a function of the two-site variance [61].

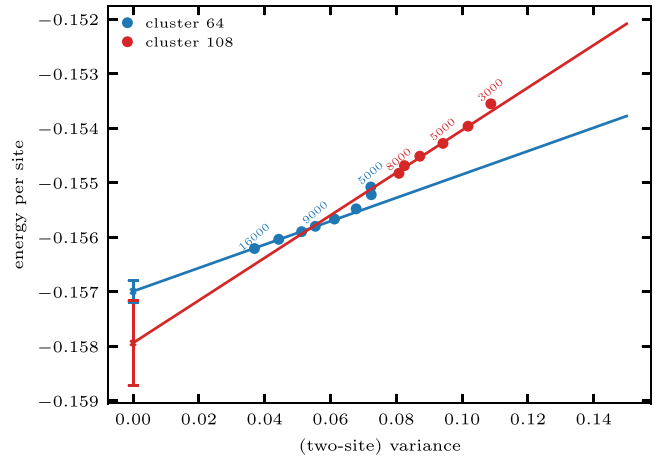

FIG. 5. The energy extrapolations (solid lines) for the 1/2 plateau state of the 64- and 108-site clusters as a function of the two-site variance. The labels indicate the corresponding U(1) bond dimensions. The last four points with the smallest variance are included in the linear fits.

To stabilize one of the magnetically ordered states in our simulation, we therefore use the pinning-field technique [59]. We apply a magnetic field (at low bond dimensions) to the same set of sites for each tetrahedral unit cell that is compatible with the polarized kagome planes such that the ordered state is stabilized. We then remove this pinning field and continue the optimization procedure while further increasing the bond dimension. With this approach the overall convergence becomes much better and smoother, as indicated in Fig. 5.

To assess the quality of the variational ground state, we compare the total energies at a fixed bond dimension $\chi = 8000$ for the 64- and 108-site clusters using different initial conditions: starting from random initial states or using the pinning-field technique to start from ordered patterns. The ordered pattern produces lower energies ($\sim 0.1J$) than starting from random initial states. We also consider another possible pattern, the R state [43], which was predicted for the $S = \frac{3}{2}$ case. This state also yields higher energies than our best variational state, although only with a small difference $\sim 0.05J$, and is therefore clearly in the low-energy manifold. The error of the extrapolated energies is defined as one quarter of the distance between the lowest-energy DMRG data point and the extrapolated value, which is commonly used in the community [67]. The same definition of the error bars is used in the main text as well and should be understood as an estimate of the systemic extrapolation error.

APPENDIX B: LOCALIZED MAGNONS IN HIGH FIELDS

Constructing analytic solutions for quantum many-body systems is a challenging discipline and succeeds only in special cases. Therefore, solutions of the ground state in the

form of quasiparticles in high fields were a huge success for spin systems in certain frustrated lattices [23–29]. Probably the most famous example of these quasiparticles is independent and localized magnon excitations in the two-dimensional kagome lattice.

Kagome lattice. Localized magnon excitations describe the ground state of the Heisenberg model in a large external field on the kagome lattice. These are confined to nontouching hexagons such that the description can be limited to a single star of David. Starting from the fully polarized state $|\uparrow\cdots\uparrow\rangle$, a single magnon state is given by (up to normalization)

$$|m\rangle \propto \sum_{j\in\hexagon} (-1)^j S_j^-|\uparrow\cdots\uparrow\rangle, \tag{B1}$$

where j runs over the hexagon. The localization can be easily verified since each corner spin of the star is attached to two spins of the inner hexagon. The contributions of flipped spins propagating to corner sites are canceled due the alternating signs. Hence, the magnetic excitation remains within the hexagon and preserves the alternating sign structure such that the hopping contribution is diagonal. Not only are the magnons localized, but they are also ground states of the Heisenberg antiferromagnet for high fields. For simplification we set $h = 0$ and focus on the hopping $H_\pm$ and interaction term H_z individually:

$$\begin{aligned} H &= JH_\pm + JH_z \\ &= \frac{J}{2}\sum_{\langle i,j\rangle}[\sigma_i^+\sigma_j^- + \sigma_i^-\sigma_j^+] + \frac{J}{4}\sum_{\langle i,j\rangle}\sigma_i^z\sigma_j^z. \end{aligned} \tag{B2}$$

Within the hexagon, the sign of each term in Eq. (B1) is inverted by $H_\pm$. Hence, $H_\pm|m\rangle = -J|m\rangle$, and the hopping term reduces the energy by J. In the kagome lattice, each site is attached to four other sites. The contribution to the energy by the interaction H_z due to a single spin flip is a reduction of $2J$, in contrast to the fully polarized state. In total, a single magnon reduces the energy by $3J$.

Due to the localization, multiple independent states can be placed within the kagome lattice as long as they are separated by at least one site. In this manner, each hexagon is uniquely assigned to nine sites in the kagome lattice to achieve the densest filling. The complete tiling of hexagons describes the ground state and corresponds to a magnetization of $m/m_{\rm sat} = 7/9$. The energy per site is reduced to $E_{7/9} = 1/6J$ from the fully polarized state $E_1 = 1/2J$.

Pyrochlore lattice. The tetrahedral unit cell of the pyrochlore lattice consist of four sites. Each face of this tetrahedron defines one out of four orientations of parallel kagome planes in the lattice. The apex spins form a separating triangular plane between the kagome planes. Equivalent to the two-dimensional case, the same formalism can be used to generate localized magnons in the pyrochlore lattice. As visualized in Fig. 6 by the red dotted triangles, nine sites are uniquely assigned to each localized hexagon in the kagome plane (black sites), such that no supercells are sharing the same site. The corresponding magnon excitation is illustrated by the red circles. Red and blue sites correspond to the upper and lower separating triangular layers, respectively. In addition to the nine sites lying inside the plane, we include the three (red) sites from the upper layer to realize a complete tiling of the pyrochlore lattice. As in the purely two-dimensional case, a localized magnon is confined to three unit cells. Hence, each magnon is assigned to 12 sites, and the corresponding plateau is $m/m_{\rm sat} = 5/6$.

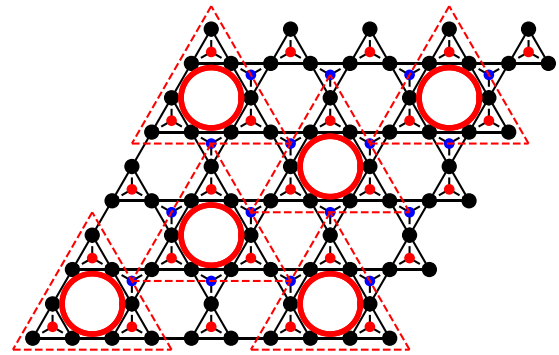

FIG. 6. Complete hexagon tiling in a single kagome plane (black sites) of the pyrochlore lattice. Red and blue sites correspond to the upper and lower separating layers, respectively. Possible localized magnon states on the corresponding hexagons are illustrated with red circles. All sites are uniquely assigned to one localized hexagon within the red triangles.

We can determine the saturation field analytically by comparing the energy per site of the fully polarized state, $E_1 = \frac{3}{4}J - \frac{h}{2}$, with the energy of the magnon crystal, $E_{5/6} = \frac{5}{12}J - \frac{5}{6}\frac{h}{2}$. The first part is derived from the Heisenberg Hamiltonian in Eq. (B1), and the second part is the energy shift induced by the external field,

$$E_1(h_{\rm sat}) = E_{5/6}(h_{\rm sat}), \tag{B3}$$

$$\frac{3}{4}J - \frac{h_{\rm sat}}{2} = \frac{5}{12}J - \frac{5}{6}\frac{h_{\rm sat}}{2} \Rightarrow h_{\rm sat} = 4J \tag{B4}$$

[1] S. V. Isakov, K. Gregor, R. Moessner, and S. L. Sondhi, Dipolar Spin Correlations in Classical Pyrochlore Magnets, Phys. Rev. Lett. **93**, 167204 (2004).

[2] C. L. Henley, Power-law spin correlations in pyrochlore antiferromagnets, Phys. Rev. B **71**, 014424 (2005).

[3] C. L. Henley, The "Coulomb phase" in frustrated systems, Annu. Rev. Condens. Matter Phys. **1**, 179 (2010).

[4] R. Moessner and J. T. Chalker, Properties of a Classical Spin Liquid: The Heisenberg Pyrochlore Antiferromagnet, Phys. Rev. Lett. **80**, 2929 (1998).

[5] M. J. Harris, S. T. Bramwell, D. F. McMorrow, T. Zeiske, and K. W. Godfrey, Geometrical Frustration in the Ferromagnetic Pyrochlore $Ho_2Ti_2O_7$, Phys. Rev. Lett. **79**, 2554 (1997).

[6] S. T. Bramwell and M. J. P. Gingras, Spin ice state in frustrated magnetic pyrochlore materials, Science **294**, 1495 (2001).

[7] C. Castelnovo, R. Moessner, and S. L. Sondhi, Magnetic monopoles in spin ice, Nature (London) **451**, 42 (2008).

[8] C. Castelnovo, R. Moessner, and S. L. Sondhi, Spin ice, fractionalization, and topological order, Annu. Rev. Condens. Matter Phys. **3**, 35 (2012).

[9] A. B. Harris, A. J. Berlinsky, and C. Bruder, Ordering by quantum fluctuations in a strongly frustrated Heisenberg antiferromagnet, J. Appl. Phys. **69**, 5200 (1991).

[10] H. Tsunetsugu, Spin-singlet order in a pyrochlore antiferromagnet, Phys. Rev. B **65**, 024415 (2001).

[11] H. Tsunetsugu, Antiferromagnetic quantum spins on the pyrochlore lattice, J. Phys. Soc. Jpn. **70**, 640 (2001).

[12] M. Isoda and S. Mori, Valence-bond crystal and anisotropic excitation spectrum on 3-dimensionally frustrated pyrochlore, J. Phys. Soc. Jpn. **67**, 4022 (1998).

[13] B. Canals and C. Lacroix, Pyrochlore Antiferromagnet: A Three-Dimensional Quantum Spin Liquid, Phys. Rev. Lett. **80**, 2933 (1998).

[14] E. Berg, E. Altman, and A. Auerbach, Singlet Excitations in Pyrochlore: A Study of Quantum Frustration, Phys. Rev. Lett. **90**, 147204 (2003).

[15] J. H. Kim and J. H. Han, Chiral spin states in the pyrochlore Heisenberg magnet: Fermionic mean-field theory and variational monte carlo calculations, Phys. Rev. B **78**, 180410(R) (2008).

[16] F. J. Burnell, S. Chakravarty, and S. L. Sondhi, Monopole flux state on the pyrochlore lattice, Phys. Rev. B **79**, 144432 (2009).

[17] Y. Iqbal, T. Müller, P. Ghosh, M. J. P. Gingras, H. O. Jeschke, S. Rachel, J. Reuther, and R. Thomale, Quantum and Classical Phases of the Pyrochlore Heisenberg Model with Competing Interactions, Phys. Rev. X **9**, 011005 (2019).

[18] E. M. Smith *et al.*, Case for a $U(1)_\pi$ Quantum Spin Liquid Ground State in the Dipole-Octupole Pyrochlore $Ce_2Zr_2O_7$, Phys. Rev. X **12**, 021015 (2022).

[19] I. Hagymási, R. Schäfer, R. Moessner, and D. J. Luitz, Possible Inversion Symmetry Breaking in the $S = \frac{1}{2}$ Pyrochlore Heisenberg Magnet, Phys. Rev. Lett. **126**, 117204 (2021).

[20] R. Schäfer, I. Hagymási, R. Moessner, and D. J. Luitz, Pyrochlore $S = \frac{1}{2}$ Heisenberg antiferromagnet at finite temperature, Phys. Rev. B **102**, 054408 (2020).

[21] N. Astrakhantsev, T. Westerhout, A. Tiwari, K. Choo, A. Chen, M. H. Fischer, G. Carleo, and T. Neupert, Broken-Symmetry Ground States of the Heisenberg Model on the Pyrochlore Lattice, Phys. Rev. X **11**, 041021 (2021).

[22] R. Moessner, Unconventional magnets in external magnetic fields, J. Phys.: Conf. Ser. **145**, 012001 (2009).

[23] *Quantum Magnetism*, edited by U. Schollwöck, J. Richter, D. J. J. Farnell, and R. F. Bishop, Lecture Notes in Physics, Vol. 645 (Springer, Berlin, 2004).

[24] A. Honecker, J. Schulenburg, and J. Richter, Magnetization plateaus in frustrated antiferromagnetic quantum spin models, J. Phys.: Condens. Matter **16**, S749 (2004).

[25] J. Schnack, H.-J. Schmidt, A. Honecker, J. Schulenburg, and J. Richter, Exact eigenstates of highly frustrated spin lattices probed in high fields, J. Phys.: Conf. Ser. **51**, 43 (2006).

[26] O. Derzhko, J. Richter, A. Honecker, and H.-J. Schmidt, Universal properties of highly frustrated quantum magnets in strong magnetic fields, Low Temp. Phys. **33**, 745 (2007).

[27] S. Nishimoto, N. Shibata, and C. Hotta, Controlling frustrated liquids and solids with an applied field in a kagome Heisenberg antiferromagnet, Nat. Commun. **4**, 2287 (2013).

[28] J. Schulenburg, A. Honecker, J. Schnack, J. Richter, and H.-J. Schmidt, Macroscopic Magnetization Jumps due to Independent Magnons in Frustrated Quantum Spin Lattices, Phys. Rev. Lett. **88**, 167207 (2002).

[29] A. Honecker, D. C. Cabra, M. D. Grynberg, P. C. W. Holdsworth, P. Pujol, J. Richter, D. Schmalfuß, and J. Schulenburg, Ground state and low-lying excitations of the spin-$\frac{1}{2}$ XXZ model on the kagomé lattice at magnetization $\frac{1}{3}$, Phys. B (Amsterdam, Neth.) **359–361**, 1391 (2005).

[30] T. Sakai and H. Nakano, Critical magnetization behavior of the triangular- and kagome-lattice quantum antiferromagnets, Phys. Rev. B **83**, 100405(R) (2011).

[31] S. Capponi, O. Derzhko, A. Honecker, A. M. Läuchli, and J. Richter, Numerical study of magnetization plateaus in the spin-$\frac{1}{2}$ kagome Heisenberg antiferromagnet, Phys. Rev. B **88**, 144416 (2013).

[32] S. Capponi, Numerical study of magnetization plateaus in the spin-$\frac{1}{2}$ Heisenberg antiferromagnet on the checkerboard lattice, Phys. Rev. B **95**, 014420 (2017).

[33] H. Nakano and T. Sakai, Anomalous behavior of the magnetization process of the s = 1/2 kagome-lattice Heisenberg antiferromagnet at one-third height of the saturation, J. Phys. Soc. Jpn. **83**, 104710 (2014).

[34] J. Schnack, J. Schulenburg, and J. Richter, Magnetism of the $n = 42$ kagome lattice antiferromagnet, Phys. Rev. B **98**, 094423 (2018).

[35] X. Plat, T. Momoi, and C. Hotta, Kinetic frustration induced supersolid in the $s = \frac{1}{2}$ kagome lattice antiferromagnet in a magnetic field, Phys. Rev. B **98**, 014415 (2018).

[36] S. Pal and S. Lal, Magnetization plateaus of the quantum pyrochlore Heisenberg antiferromagnet, Phys. Rev. B **100**, 104421 (2019).

[37] K. Penc, N. Shannon, and H. Shiba, Half-Magnetization Plateau Stabilized by Structural Distortion in the Antiferromagnetic Heisenberg Model on a Pyrochlore Lattice, Phys. Rev. Lett. **93**, 197203 (2004).

[38] H. Ueda, H. A. Katori, H. Mitamura, T. Goto, and H. Takagi, Magnetic-Field Induced Transition to the $\frac{1}{2}$ Magnetization Plateau State in the Geometrically Frustrated Magnet $CdCr_2O_4$, Phys. Rev. Lett. **94**, 047202 (2005).

[39] E. Kojima, A. Miyata, Y. Motome, H. Ueda, Y. Ueda, and S. Takeyama, Magnetic orders of highly frustrated spinel, $ZnCr_2O_4$ in magnetic fields up to 400 T, J. Low Temp. Phys. **159**, 3 (2010).

[40] K. Matsuhira, Z. Hiroi, T. Tayama, S. Takagi, and T. Sakakibara, A new macroscopically degenerate ground state in the spin ice compound $Dy_2Ti_2O_7$ under a magnetic field, J. Phys.: Condens. Matter **14**, L559 (2002).

[41] M. Udagawa, M. Ogata, and Z. Hiroi, Exact result of ground-state entropy for ising pyrochlore magnets under a magnetic field along [111] axis, J. Phys. Soc. Jpn. **71**, 2365 (2002).

[42] R. Moessner and S. L. Sondhi, Theory of the [111] magnetization plateau in spin ice, Phys. Rev. B **68**, 064411 (2003).

[43] D. L. Bergman, R. Shindou, G. A. Fiete, and L. Balents, Quantum Effects in a Half-Polarized Pyrochlore Antiferromagnet, Phys. Rev. Lett. **96**, 097207 (2006).

[44] M. E. Zhitomirsky and H. Tsunetsugu, Lattice gas description of pyrochlore and checkerboard antiferromagnets in a strong magnetic field, Phys. Rev. B **75**, 224416 (2007).

[45] M. E. Zhitomirsky, A. Honecker, and O. A. Petrenko, Field Induced Ordering in Highly Frustrated Antiferromagnets, Phys. Rev. Lett. **85**, 3269 (2000).

[46] T. Coletta, M. E. Zhitomirsky, and F. Mila, Quantum stabilization of classically unstable plateau structures, Phys. Rev. B **87**, 060407(R) (2013).

[47] X. Chen, S.-J. Ran, T. Liu, C. Peng, Y.-Z. Huang, and G. Su, Thermodynamics of spin-1/2 kagomé Heisenberg antiferromagnet: Algebraic paramagnetic liquid and finite-temperature phase diagram, Sci. Bull. **63**, 1545 (2018).

[48] H. Nakano and T. Sakai, Numerical-diagonalization study of magnetization process of frustrated spin-1/2 Heisenberg antiferromagnets in two dimensions: -Triangular- and kagome-lattice antiferromagnets-, J. Phys. Soc. Jpn. **87**, 063706 (2018).

[49] K. W. Plumb, H. J. Changlani, A. Scheie, S. Zhang, J. W. Krizan, J. A. Rodriguez-Rivera, Y. Qiu, B. Winn, R. J. Cava, and C. L. Broholm, Continuum of quantum fluctuations in a three-dimensional S = 1 Heisenberg magnet, Nat. Phys. **15**, 54 (2019).

[50] C. Hubig, F. Lachenmaier, N.-O. Linden, T. Reinhard, L. Stenzel, A. Swoboda, and M. Grundner, The SYTEN toolkit, https://syten.eu/.

[51] C. Hubig, Symmetry-protected tensor networks, Ph.D. thesis, Ludwig-Maximilians-Universität München, 2017.

[52] C. Hubig, I. P. McCulloch, U. Schollwöck, and F. A. Wolf, Strictly single-site DMRG algorithm with subspace expansion, Phys. Rev. B **91**, 155115 (2015).

[53] I. P. McCulloch, From density-matrix renormalization group to matrix product states, J. Stat. Mech. (2007) P10014.

[54] S. R. White, Density Matrix Formulation for Quantum Renormalization Groups, Phys. Rev. Lett. **69**, 2863 (1992).

[55] S. R. White, Density-matrix algorithms for quantum renormalization groups, Phys. Rev. B **48**, 10345 (1993).

[56] R. M. Noack, S. R. Manmana, A. Avella, and F. Mancini, Diagonalization- and numerical renormalization-group-based methods for interacting quantum systems, in *Lectures on the Physics of Highly Correlated Electron Systems IX: Ninth Training Course in the Physics of Correlated Electron Systems and High-*T_c *Superconductors*, AIP Conf. Proc. No. 789 (AIP, Melville, NY, 2005), p. 93.

[57] U. Schollwöck, The density-matrix renormalization group in the age of matrix product states, Ann. Phys. (NY) **326**, 96 (2011).

[58] K. A. Hallberg, New trends in density matrix renormalization, Adv. Phys. **55**, 477 (2006).

[59] E. M. Stoudenmire and S. R. White, Studying two-dimensional systems with the density matrix renormalization group, Annu. Rev. Condens. Matter Phys. **3**, 111 (2012).

[60] J. Ummethum, J. Schnack, and A. M. Läuchli, Large-scale numerical investigations of the antiferromagnetic Heisenberg icosidodecahedron, J. Magn. Magn. Mater. **327**, 103 (2013).

[61] C. Hubig, J. Haegeman, and U. Schollwöck, Error estimates for extrapolations with matrix-product states, Phys. Rev. B **97**, 045125 (2018).

[62] L. Vanderstraeten, B. Vanhecke, and F. Verstraete, Residual entropies for three-dimensional frustrated spin systems with tensor networks, Phys. Rev. E **98**, 042145 (2018).

[63] J. F. Nagle, Lattice statistics of hydrogen bonded crystals. I. The residual entropy of ice, J. Math. Phys. **7**, 1484 (1966).

[64] J. F. Nagle, New series-expansion method for the dimer problem, Phys. Rev. **152**, 190 (1966).

[65] R. Moessner, Relief and generation of frustration in pyrochlore magnets by single-ion anisotropy, Phys. Rev. B **57**, R5587 (1998).

[66] C. Hubig, I. P. McCulloch, and U. Schollwöck, Generic construction of efficient matrix product operators, Phys. Rev. B **95**, 035129 (2017).

[67] B.-X. Zheng, C.-M. Chung, P. Corboz, G. Ehlers, M.-P. Qin, R. M. Noack, H. Shi, S. R. White, S. Zhang, and G. K.-L. Chan, Stripe order in the underdoped region of the two-dimensional Hubbard model, Science **358**, 1155 (2017).